Research Square

Preprints are preliminary reports that have not undergone peer review.
They should not be considered conclusive, used to inform clinical practice,
or referenced by the media as validated information.

Determining the Presence of a Stress-Free State in Panel Paintings Through Numerical Modeling and Experimental Tests on Historical Artworks

Lorenzo Riparbelli
DAGRI, Università di Firenze
Łukasz Bratasz
Polish Academy of Sciences
Michał Łukomski
Getty Conservation Institute
Paola Mazzanti
paola.mazzanti@unifi.it

DAGRI, Università di Firenze
Luciano Ricciardi
Opificio delle Pietre Dure
Sandra Rossi
Opificio delle Pietre Dure
Ciro Castelli
Opificio delle Pietre Dure
Andrea Santacesaria
Opificio delle Pietre Dure
Marco Fioravanti
DAGRI, Università di Firenze

Article

Keywords: panel paintings; zero-stress level; hygro-mechanical modelling; inverse identification; deep cracks; acclimatization; museum climate

Posted Date: October 8th, 2026

DOI: https://doi.org/10.21203/rs.3.rs-11082478/v1

License: This work is licensed under a Creative Commons Attribution 4.0 International License.
Read Full License

Additional Declarations: No competing interests reported.

Determining the Presence of a Stress-Free State in Panel Paintings Through Numerical Modeling and Experimental Tests on Historical Artworks

Lorenzo Riparbelli[1,2], Łukasz Bratasz[3], Michał Łukomski[2], Paola Mazzanti[1*], Luciano Ricciardi[4], Sandra Rossi[4], Ciro Castelli[4], Andrea Santacesaria[4], Marco Fioravanti[1]

[1] DAGRI, Università di Firenze, Florence, Italy

[2] Science Department, Getty Conservation Institute, Los Angeles, USA

[3] Jerzy Haber Institute of Catalysis and Surface Chemistry Polish Academy of Sciences, Kraków, Poland

4 Opificio delle Pietre Dure, Florence, Italy

*Corresponding author: Paola Mazzanti paola.mazzanti@unifi.it

ABSTRACT

Museum environmental guidelines rest on a largely untested assumption: that artworks reach a stress-free state at the long-term average relative humidity (RH) of their environment — a premise that underpins the assessment of climate-induced mechanical damage. This work demonstrates the existence of such a state, here termed the zero-stress level (ZSL): the moisture content at which stress in the paint layer is minimized. Deformation histories of historical wooden panel paintings, recorded under controlled RH cycling, are interpreted through a coupled hygro-mechanical finite-element model combined with inverse identification. The model introduces a damage-based constitutive law for the paint layer, whose stiffness differs between crack-open (tension) and crack-closed (compression) states; this asymmetry renders the ZSL observable, non-invasively, as a difference between the adsorption and desorption responses. In paintings whose decorative layer bears deep cracks — cracking, lifting and loss of adhesion of the paint layers — the identified ZSL falls within the range of the long-term average storage RH, providing quantitative evidence of acclimatization, whereas paintings with only superficial craquelure show a symmetric response that leaves the ZSL undetectable. These findings substantiate the silent assumption behind museum guidelines of acclimatization.

Keywords: panel paintings; zero-stress level; hygro-mechanical modelling; inverse identification; deep cracks; acclimatization; museum climate

1. INTRODUCTION

The first models for assessing moisture-induced physical damage to vulnerable museum objects were developed in the early 1990s. They used the mechanical properties of historic and artistic materials based on experimental measurements and assumed that the materials were uniformly restrained [1–4]. A particularly relevant group of objects is panel paintings due to their significant artistic value and high vulnerability to environmental variations [5–8]. An analysis carried out on scientific literature suggests that RH variations of approximately ±10% around 50% RH do not generate stresses exceeding the elastic limits of the materials and therefore could be considered safe [9]. When the object is stored in the environment exceeding the safe range, damage may and

often does occur. The RH ranges determined were only slightly refined through finite element (FEM) modeling [10] allowing to account for sorption hysteresis, moisture diffusion and ability of painting to deform. The development in FE modeling and inverse engineering methods led to a precise physical interpretation of an extensive experimental monitoring of historical panel paintings. The study highlighted the inherent variability of wood and paint layers as well as complex, strongly non-linear behavior[11, 12]. All of the above analysis - analytical or numerical – were usually carried out under two assumptions. First, all materials constituting the painting are undamaged. Second, those materials are in a stress-free state at certain environmental conditions. Both assumptions have a significant impact on the allowable RH variations determined, and both are related to the acclimatization of objects, to the environment in which they are stored.

There are numerous observations indicating that objects acclimatize to the environment in which they are stored [13]. The primary mechanism by which objects acclimatize to unstable environment is formation of material and structural damage that leads to relaxation of environmental stresses. In the case of panel paintings, Bratasz and Sereshk quantitatively demonstrated how the development of deep cracks in the paint layer leads to redistribution and reduction of stress [14]. In historical objects such cracks are largely inherited from the past: they have accumulated over centuries under uncontrolled climates, and often also under rigid restraint systems and past interventions, through handling and relocation, and because of object-specific features of the support and defects at the interfaces between support, glue, canvas and ground. The damage state of a painting thus reflects its whole climatic and mechanical history [5, 15]. Beyond cracking, several complementary mechanisms contribute to stress evolution. Exceeding the elastic limit induces plastic deformation and shifts the material's stress-free state. The time-dependent phenomena - viscoelasticity and viscoplasticity - in both wood and paint layers progressively reduce internal stresses by molecular-level rearrangements of polymer chains when deformation is maintained [16, 17]. The effect is enhanced by mechano-sorptive creep in wood that couples mechanical deformation to moisture content changes under load, providing a further pathway for stress redistribution during RH variations [18, 19]. All these mechanisms are the main drivers of energy dissipation in the "panel painting" system; they are interconnected and interact in a nonlinear relationship, and they may shift object toward a new equilibrium in which the paint layer remains stress-free. This introduces the term hereinafter referred to as the zero-stress level (ZSL), defined as a specific RH, or more precisely, moisture content (MC) of materials, at which the stress in the paint layer is minimized, also for the effects of damage caused by critical conservation conditions that may have affected the artwork over the course of its history. The relation between RH and MC is adopted from [11].

The environmental guidelines for museums have evolved over the years from prescribing a single optimal RH level of 50% or 55% toward recommending RH levels corresponding to the historical average RH. These recommendations are based on observations by object owners and a general understanding of material behavior, which assume that the ZSL corresponds to the long-term average RH. Two widely used environmental guidelines - the ASHRAE guidelines [20] and the European standard EN 15757:2010 [21, 22] - define the concept of the "historic climate" and explicitly recommend long-term RH average as

the level at which objects are stress free. However, there is no experimental data as to whether and to what extent this assumption holds.

The aim of this study is to demonstrate the existence of a "stress-free" state in paintings and identify the corresponding RH level by using computer modeling to interpret results of an experiment conducted on a set of historic paintings [11, 12]. In the following sections, a computational model is presented and used to interpret the recorded deformations of historical paintings subjected to repeated RH cycles. The purpose is to interpret a specific experimental evidence on six paintings, not to provide a general explanation of how and why cracks form in panel paintings; the factors that produced the cracks observed in each work lie beyond the scope of this study. Computational models were used to interpret the results of an experiment carried out on a series of historical paintings [11, 12, 23]. The study aims to demonstrate that ageing phenomena occurring over time can lead to the establishment of a 'stress-free' state in the paintings and to determine the relative humidity (RH) level corresponding to zero stress.

2. MATERIALS AND METHODS

2.1 *Experimental study of historic panel paintings behavior*

A detailed description of the experimental tests on the six historic panel paintings, belonging to different Florentine schools, together with the criteria guiding their selection and the testing methodology, can be found in [11, 12, 23]. Of relevance here, WPP1 and WPP3 are painted on a canvas interlayer glued between the wooden support and a gesso ground.

The six paintings, all made of poplar wood (*Populus alba L.*), were placed in a climatic chamber constructed at the Opificio delle Pietre Dure (OPD), in which RH varied between 53% and 60% RH through controlled step changes. Since the study focused on the properties and changes of the paint layer, the painted surface was waterproofed with an aluminum foil, with no axial or bending rigidity, to remove the surface emissivity variable from the analysis. The foil was applied and removed by the OPD conservators under their direct supervision. Like the RH cycling itself, kept within a narrow range, it is a non-invasive procedure: it is not involved in the generation of the deep cracks discussed in Section 2.2. Additionally, the crossbars were detached from the paintings during testing to simplify the response of the panels and ease the interpretation of the results; they are restoration crossbars made according to the OPD method, held to the panel by spring-loaded connectors on wooden anchoring buttons, which allow them to be detached and refitted reversibly without any intervention on the original support [15, 23]. The deformation - cupping and elongation - of each painting was measured using a Deformometric Kit (DK) [24], a device consisting of two metal columns fixed to the back face of the panel, connected by two displacement transducers at different heights (upper and lower measurement lines). As the panel deforms in response to RH changes, the relative displacement between the columns is recorded, from which the cupping angle is derived. This parameter provides a direct measure of the panel's transverse deformation. The direction of cupping change is opposite during sorption and desorption of moisture, but the magnitude and dynamics of the change are expected to be the same for equivalent increases and decreases in MC. Figure 1 shows the absolute change in cupping angle for

six paintings during a single humidity cycle (adsorption from 53% to 60% RH and desorption from 60% to 53% RH, corresponding to MC changes of approximately +0.59 and −0.63 percentage points, respectively, calculated according to the methods discussed in [11]). For comparison, the desorption responses were multiplied by 0.59/0.63, so that both responses refer to an MC change of 0.59 percentage points.

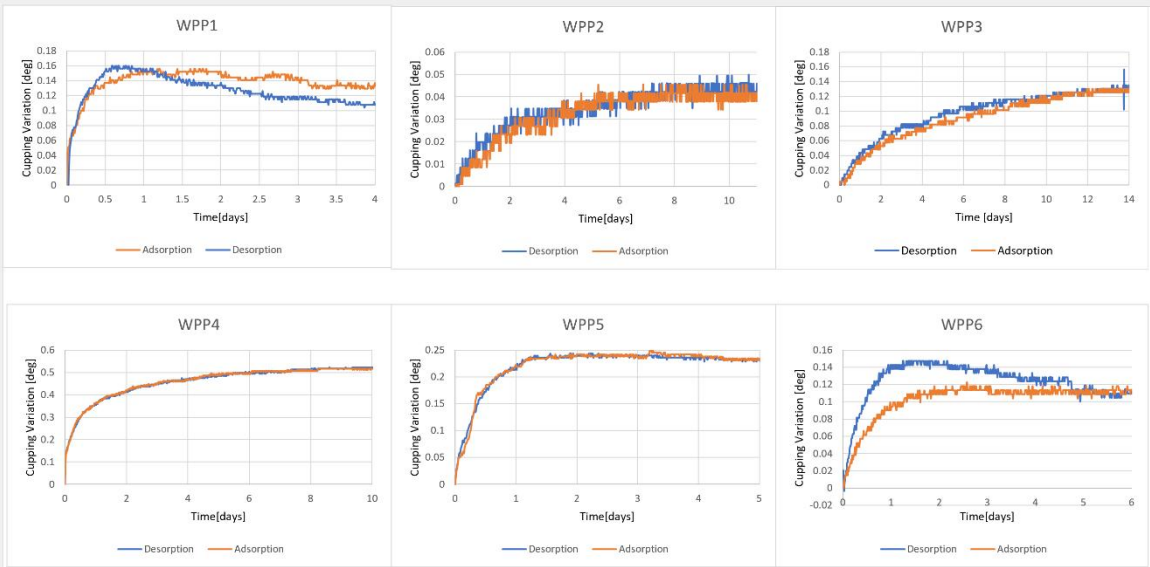


Figure 1. Changes in the cupping angle for six paintings exposed to a 53–60% RH cycle. Note that the panel deformation during adsorption and desorption is opposite; therefore, for comparison, the absolute value of the cupping angle is presented (results obtained during adsorption are reflected through zero). Desorption responses are scaled by 0.59/0.63 to match the MC change during adsorption.

Three paintings (WPP2, WPP4, WPP5) show similar deformations during sorption and desorption, whereas WPP1, WPP3, and WPP6 exhibit markedly different behaviors.

After scaling adsorption and desorption responses to the same MC change, we hypothesize that the observed asymmetry in the paintings' behavior arises from differences in the stiffness of the decorative layer (ground and paint layer) during these processes, consistently with the analysis presented in [11]. We further examine how this stiffness difference is related to the presence of deep cracks in the paint layer.

2.2 Panel deformation, craquelure and deep cracks

Moisture-induced cracking in decorative layer results from the mismatch in hygric response between the wooden substrate and the decorative layer [3, 9, 25]. Composed of brittle materials such as animal glue-based ground, tempera, or aged oil paints and varnish, the decorative layer cannot fully accommodate the wood expansion or contraction [16, 25–27]. RH changes generate tensile and compressive stresses in the

decorative layer, and when these stresses exceed the material's tensile strength, cracking occurs [25]. Once initiated, these cracks act as new sites of stress concentration, promoting further cracking over time during repeated RH cycles. Depending on the materials used, painting structure, and historic pattern of environmental variations over the years, a distinctive crack patterns form [28]. The severity of this mechanism increases with the thickness of the ground and of the glue layers [25]. Hygric mismatch is, however, not the only source of cracking in historical panels: rigid restraint systems and past interventions, acting in combination with environmental variations, handling and transport, and with the specific features of each support — the cut of the boards, the quality of the ground — can generate cracks whose specific causes are complex and object-dependent. In most historical paintings the bulk of this cracking developed in the past, under uncontrolled climates and rigid restraint systems, and is therefore already present when the object enters a controlled environment.

The term craquelure refers to the network of cracks, of various topologies and depths, visible on the painted surface. Craquelure and deep cracks of the decorative layer are two different phenomena, and in this work they are kept distinct. Craquelure is a surface phenomenon, largely confined to the upper paint and varnish layers, resulting from their natural shrinkage during drying and ageing. The term deep cracks is used here in the broad sense of any loss of continuity of the decorative layer that runs through the ground layers — cracks proper, lifted and detached paint, filled losses, loss of adhesion between ground and support, loss of cohesion between paint layers, decohesion of the ground — and that therefore opens in tension and closes in compression. Because they run through the ground, deep cracks are structural in a precise sense: they alter measurably the stiffness of the decorative layer and hence the deformation behaviour of the panel, which is what the method detects. They are the outcome of the climatic and mechanical history of each object rather than of its present environment. Only such discontinuities modify the transfer of tensile stress between the wooden support and the decorative layer. In the model (Sections 2.3–2.4) they are represented by a damage variable, in the mechanical sense of the term. What the method evaluates is thus the mechanical integrity of the paint layer — its ability to transfer stress — and not the craquelure, which is neither measured nor modelled.

The discontinuities in the decorative layer change stress transfer between layers which is manifested as an alteration of the paint layer stiffness: the paint layer continues to contribute to stiffness under compression (when cracks close) but provides little or no resistance under tension (when cracks open). The situation is illustrated conceptually in Figure 2.

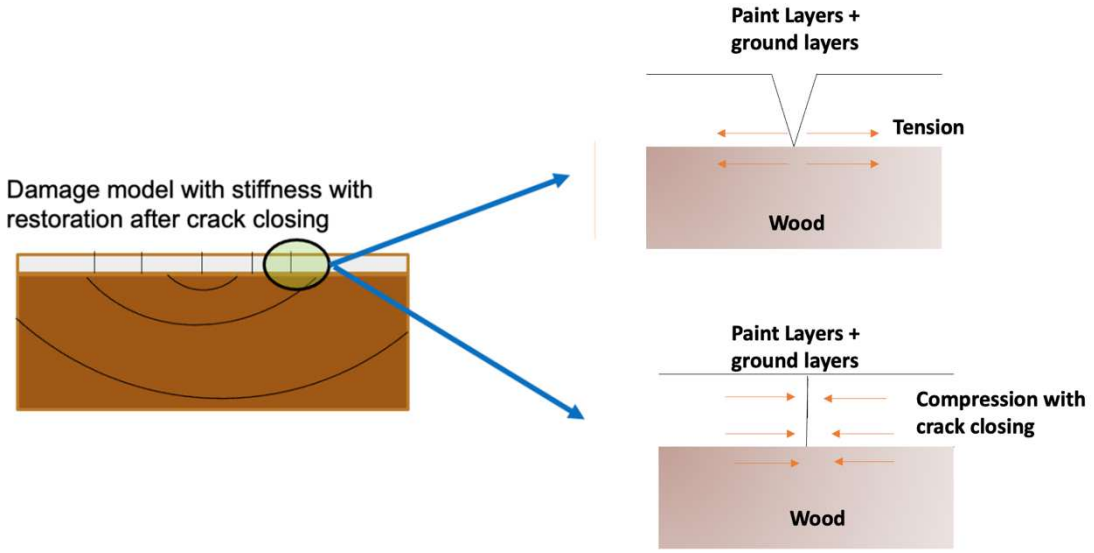


Figure 2. Effect of crack opening and closing in the decorative layer on the panel painting's resistance to compressive and tensile deformation.

During the transition between tension and compression, there is a state in which the stresses in the paint layer are zero.

In the following section, a numerical model is presented, along with a specific computational procedure implemented to interpret the experimentally observed asymmetry in the panel's response and determine the conditions of the ZSL.

2.3 Numerical model and simulation procedure

The numerical model presented here is used to interpret experimental observations of asymmetric response of panel paintings to increase and decrease in RH. It uses parameters obtained through inverse identification and values taken from literature along with simplifying assumptions —material homogeneity of the paint layer and isotropy of diffusion.

The coupled hygro-mechanical finite element model used in this study is based on the framework established in [11, 29–31]. It has been shown that it is capable of reproducing the deformation of panel paintings through inverse identification of material parameters. The present work adopts the same diffusion formulation, orthotropic wood mechanics and optimization strategy, but introduces an important extension: a damage-based constitutive law for the paint layers that distinguishes between the mechanical states of cracked and uncracked material. This key modification enables the model to capture the experimentally observed asymmetric response of panel paintings to RH variations and, through it, to identify the possible presence of the ZSL in the paint layer. An inverse

identification procedure calibrates the model against measured deformation histories, extracting the ZSL and the associated mechanical parameters for each painting.

The diffusion formulation, finite element discretization and sensitivity analysis are detailed in Annexes A and C; the constitutive law and its calibration are presented below and further developed in Annex B.

For constructing geometry and mesh discretization, we used Salome-Meca, an open-source software environment developed by Électricité de France (EDF) in collaboration with SIMVIA. Simulations were conducted using the open-source solver code_aster [32], in synergy with MFront [31, 33] that managed the cylindrical coordinates that mimic the anatomical directions in wood.

The model accounts for reduction of the effective Young's modulus of decorative layer due to crack opening when wood swells. The actual reduction is calculated as follows. When the tensile strain in decorative layer exceeds a threshold of 0.2%, it undergoes a sharp stress drop (snap-back) characteristic for brittle fracture behavior typical for gesso and aged paint. Stiffness recovers during wood shrinkage, as the decorative layer transitions from tension to compression, representing the physical mechanism by which walls of the crack come back into contact and transmit compressive loads. The model uses a strain-based damage criterion, with the paint-layer modulus identified as an effective value for the adopted layer thickness and wood stiffness (see Annex B for details and calibration criteria). The calibrated constitutive law produces the stress-strain response shown in Figure 3:

1. **Elastic phase ($\varepsilon < 0.2\%$)**: Linear response with slope E_0 (undamaged initial rigidity)
2. **Snap-back ($\varepsilon \approx 0.2\%$)**: Abrupt stress drop immediately after reaching ft (failure threshold)
3. **Softening phase ($0.2\% < \varepsilon < 0.5\%$)**: Continued stiffness degradation as damage accumulates
4. **Residual phase ($\varepsilon > 0.5\%$)**: Severely degraded response (~2% of E_0)
5. **Unloading/compression**: Near-complete stiffness recovery following the initial elastic slope

The critical strain levels of 0.2% and 0.5% used in the model are adopted from experimental works analyzing brittle cracking of gesso [27, 34].

Figure 3 illustrates how the paint layer changes from stiff (1) into softer material (2) as damage develops after reaching a critical tensile strain of 0.2%. When the strain reaches 0.5%, the material is highly damaged and the stiffness of the decorative layer becomes

negligible. In contrast, compression does not cause any damage, and the material remains stiff (cracks are closed).

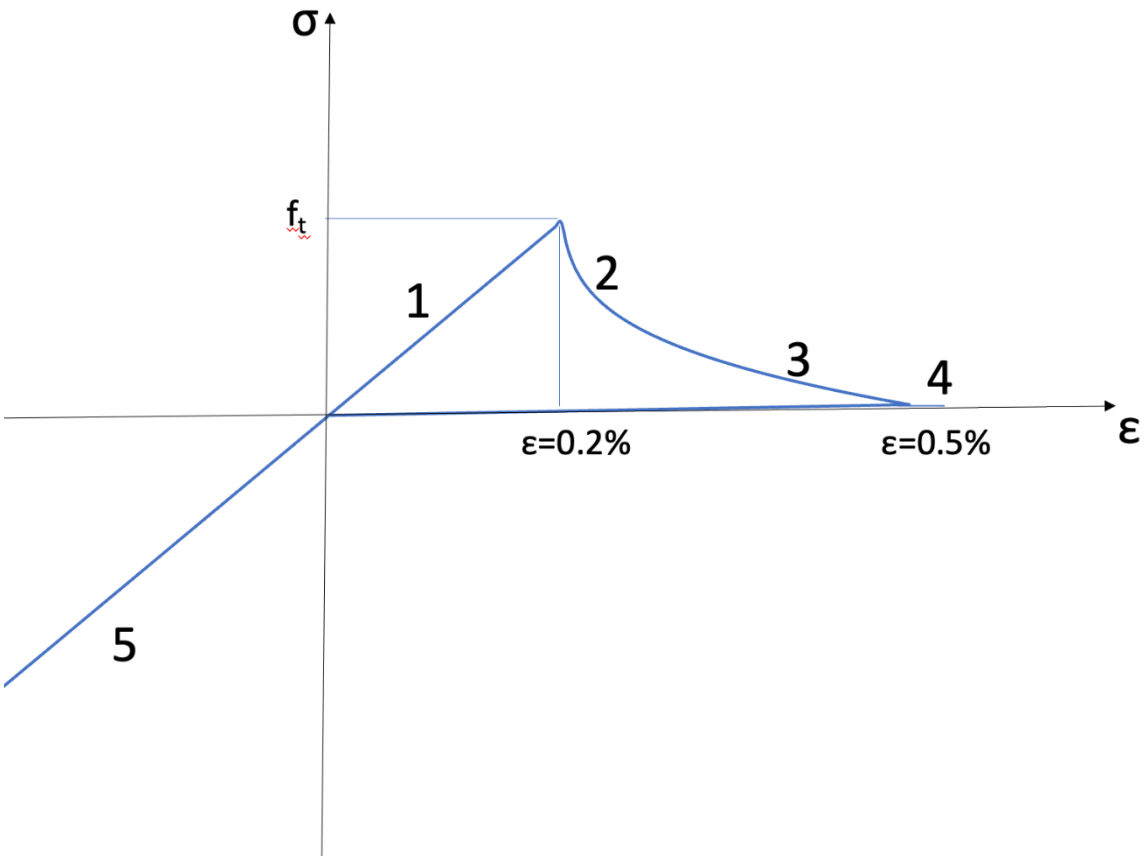


Figure 3 - Stress-Strain relation for the material law of damage taken into account for the paint layers

2.4 Numerical modeling of a paint layer damage

The state of deterioration of any historical panel painting results from a sequence of environmental events accumulated over centuries. Rather than imposing damage distribution a priori, the model builds its own damage state through a numeric procedure which generates a plausible damage distribution consistent with that observed in the paintings, mainly present in the tangential zones of the planks. The extent of damage in the decorative layer depends on the amplitude and duration of the humidity change, as well as on the geometry of the painting and the presence and configuration of any restraint crossbar system. For the configurations considered, crossbars mainly increase strain at the wood–paint interface without substantially changing its overall distribution [23]; their effect is therefore represented in the simulation by appropriately adjusting the full MC excursion of the damaging cycle.

A “damaging humidity cycle” is applied in the simulation prior to the actual RH experimental cycle imposed on the painting (Figure 4). This cycle generates damage distribution in the decorative layer [34]. Note that in Figure 4, the y-axis represents

moisture content, not RH, as the model is calibrated using moisture content, not RH. Using moisture content in the calculations avoids ambiguity associated with RH hysteresis and its dependence on temperature.

The damaging cycles are symmetrical about an imaginary axis centered at RH = 56.5%; this value is taken as the reference point for the zero stress level, and therefore all variations in MC are considered relative to this axis. The numerical optimization procedure determines the full MC excursion of the damaging cycle that produces a damage distribution, to minimize the difference between experimental observations and model predictions. In this way mechanical effects - specifically, the stiffness difference between crack-open and crack-closed states - are determined.

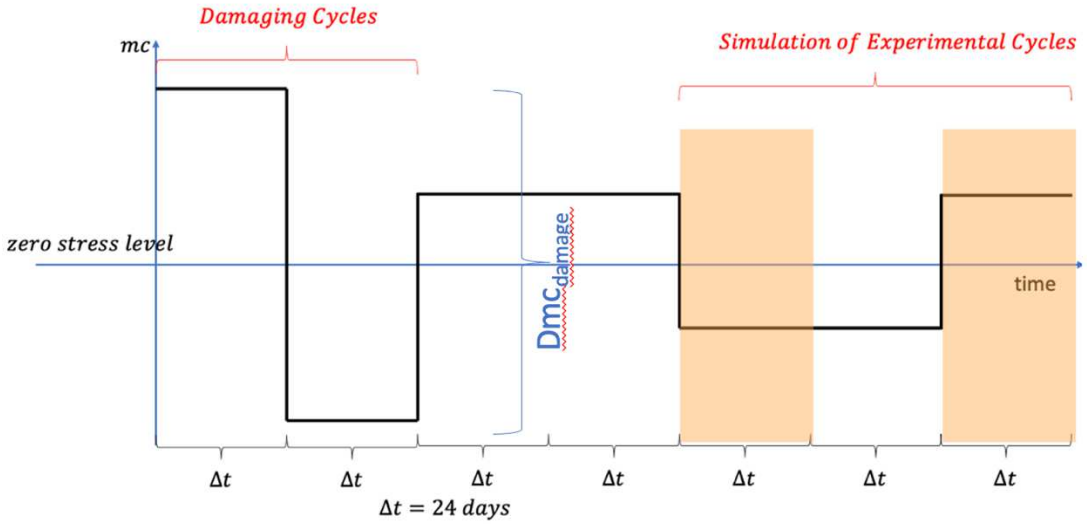


Figure 4 - The sequence of humidity changes used in the simulation; specifically the "damaging cycles" and the "experimental cycles". Orange areas indicate the time windows used for identification (see Section 2.5); Figures 1 and 6–8 display shorter excerpts of these response histories. The 24-day interval was chosen based on the experimentally observed equilibration time of the panels and it is, in general, case-dependent.

2.5 Optimization procedures

An optimization algorithm, discussed in [11, 30] and used in a similar contest, was expanded by including damaging cycle. It was used to match the simulation with experimental data, determining the hygro-mechanical parameters across all six paintings. The optimization process minimizes the norm of the difference between numerically calculated deformation time histories and measurements of shape change obtained with the Deformometric Kit. The minimization strategy combines a genetic algorithm with a subsequent Nelder–Mead optimization[11, 30]. Such a hybrid approach is well-suited to problems where small parameter variations produce large changes in model response[35, 36].

The optimization procedure focused on six key parameters:

1. *D0*: The wood diffusion coefficient
2. *Ec1*: Emissivity of the wood
3. *Ep*: Undamaged paint layer elastic modulus

4. Δmc_{damage}: The full moisture-content excursion of the damaging cycle in Figure 4, i.e., the difference between its upper and lower MC levels, expressed in percentage points (pp) of MC. This cycle generates the damage distribution in the decorative layer.
5. *X*: A scaling factor for the hygromechanical deformation tensor that combines the dimensional response coefficients along the orthotropic directions of the wood
6. *Y*: A scaling factor for the compliance tensor for wood

Although the model used in this work differs from previously used models—assuming variable stiffness rather than constant stiffness as in [11]—the underlying structure of the inverse problem remains unchanged. In both models, the same parameters are identified, and they enter the governing equations with the same functional dependence on the measured deformation (Annex C). The optimization process employs a single, continuous-time history encompassing the adsorption and desorption process. All parameters, except for the stiffness of the paint layer, remain identical. Consequently, any predicted asymmetry between adsorption and desorption arises solely from damage-induced stiffness variations, enabling identification of the transition from tension to compression in the paint layer, i.e., the ZSL.

The experimental protocol — a single cycle between 53% and 60% RH — does not provide sufficient information to independently resolve both the ZSL position and the Δmc_{damage} (Annex C). Therefore, based on experiment, one can only confirm or deny existence of ZSL within tested RH range.

Figure 5 compares the normalised cupping curves obtained when the ZSL is placed on either side of the experimental RH range. Both simulations use WPP1 and the properties identified in Section 3.1. The decorative layer is assumed to be heavily damaged throughout, retaining only 2% of its initial stiffness when the cracks are open. Adsorption runs from 53% to 60% RH, and desorption follows the reverse path.
The ZSL is set outside the moisture-content interval by an amount equal to 10% of its width: above the upper limit in Figure 5a and below the lower limit in Figure 5b, corresponding to approximately 60.7% and 52.3% RH, respectively. In Figure 5a, the panel remains drier than its stress-free state. The decorative layer is therefore compressed, its cracks remain closed and its full stiffness is maintained. In Figure 5b, the panel remains wetter than its stress-free state, leaving the cracks open and the decorative layer with a negligible contribution to panel stiffness. Neither cycle produces a change in crack state or stiffness, so the adsorption and desorption curves overlap. A decorative layer without deep cracks behaves as in Figure 5a.
Asymmetry can thus arise only if the ZSL lies within the cycled range, allowing the cracks to open and close during the test. Section 3 uses this condition to locate the ZSL of each painting. With all other parameters unchanged, the two limiting cases also recover the response patterns described in [11,12]: the stiff, closed-crack state produces the non-monotonic cupping termed flying wood, whereas the compliant, open-crack state produces monotonic cupping.

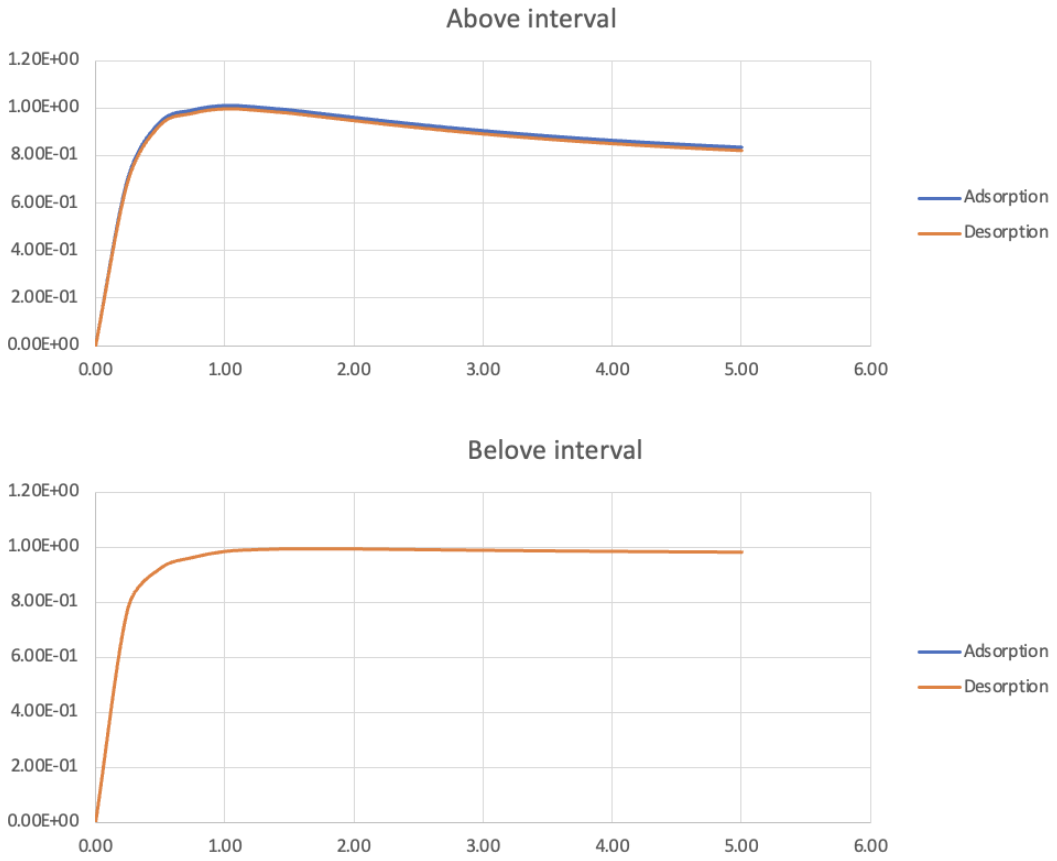


Figure 5 - Sensitivity of deformation response to ZSL position for WPP1. Normalized absolute value of curvature for adsorption and desorption in 53-60% RH for ZSL a) above 60%RH, b) below 53%RH.

3. RESULTS AND DISCUSSION

In the analysis of the results, simulations using material parameters obtained from the optimization process are compared with the experimentally measured deformations of the panels. The graphs in Figures 6–8 show the measured and calculated deformation profiles. To enable easy comparison of panel behavior during adsorption and desorption, the graphs present the absolute change in cupping angle (results obtained during adsorption are reflected through zero). Desorption responses are scaled as described in Section 2.1. The plots show excerpts of the responses to the experimental cycles in Figure 4, with time measured from the start of each experimental RH step. For the three paintings in which damage to the paint layer leads to different deformations, detailed images and high-magnification photographs illustrating the observable deep cracks of the paint layer are also presented. The spacing of these cracks varies across the painting. They are densest in the central area, where the wood is cut tangentially; the direction

most responsive to RH changes, and become more widely spaced toward the edges, where the wood is cut radially. This results in a corresponding distribution of stiffness reduction in the paint layer, with the greatest effect occurring in the central area, where cracks are most dense.

For each analyzed painting, the obtained parameters are presented and compared with those from a previous analysis that did not take into account the change in stiffness due to damage accumulation [11].

3.1 WPP1

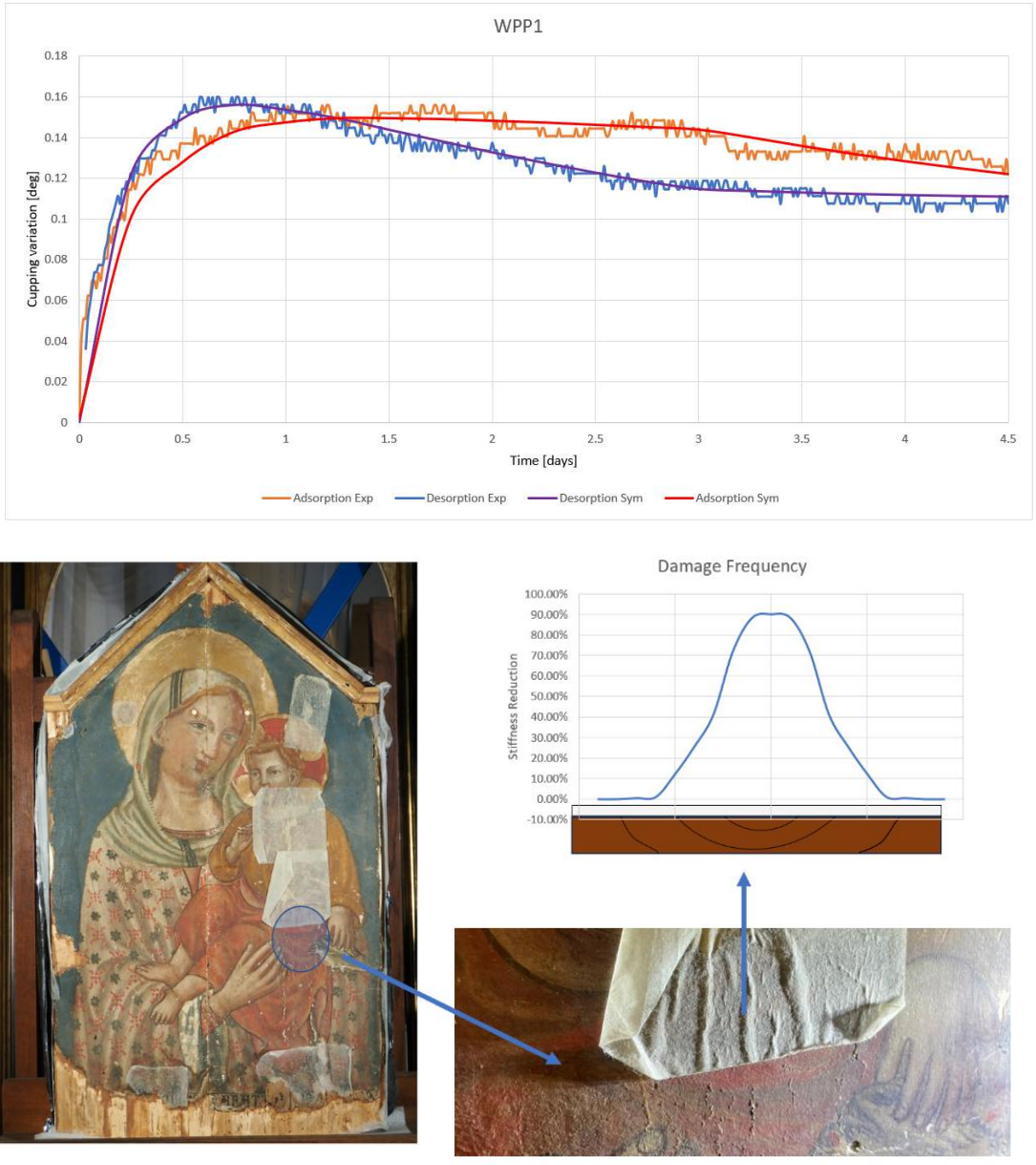


Figure 6. ***WPP1:*** *(a) Comparison of measured and simulated moisture-induced deformation of the true left side panel of the painting; (b) photo of the painting; (c) macrophotography showing cracks and lifting (tenting) of the paint layer in the central part of the panel; (d) distribution of stiffness reduction in the paint layer in the analyzed panel.*

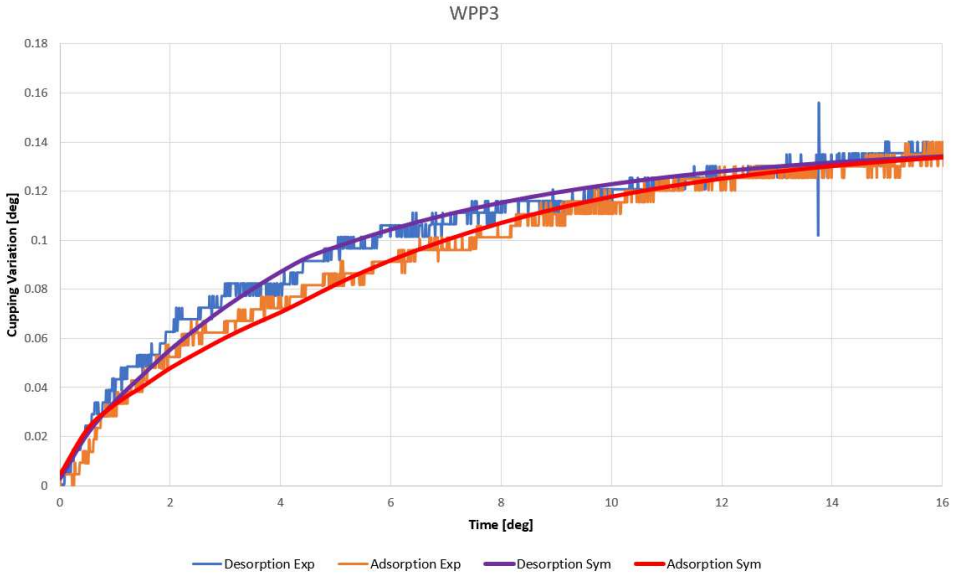
Table 1. Parameters of the simulation of WPP1 behavior. Results obtained with the model, not taking into account the influence of paint-layer cracking on paint stiffness [11], are shown for comparison.

	Δmc_{damage} [pp]	D_0 [$m^2 \cdot s^{-1}$]	$E_{p,high}$ [MPa]	E_{c1} [$m \cdot s^{-1}$]	X wp	Y
WPP1 old	x	$4.0\ 10^{-10}$	1506	$9.0\ 10^{-08}$	0.47	0.82
WPP1 damage	3.55	$3.6\ 10^{-10}$	1854	$7.9\ 10^{-08}$	0.62	0.89

Figure 6 shows an excellent agreement between the measured deformation and the computer simulations. The parameters of the current model and the previous model, which did not account for the influence of paint layer cracking on stiffness, are presented in Table 1. The results indicate that the ZSL lies in the range of 53–60% RH. The cracking of the paint layer results from $\Delta mc_{damage} = 3.55$ (Table 1).

The "undamaged" paint layer modulus was determined to be $E_0 = 1854$MPa. The damage distribution, shown as the spatial variation of stiffness reduction (Figure 6d), indicates that damage is most severe in the central part of the analyzed panel. This finding was confirmed by visual inspection of the painting, which revealed deep vertical cracks in the paint layer accompanied by visible lifting. In the central area, these cracks have weakened the paint layer to the extent that stabilization with Japanese tissue facing is necessary.

3.2 WPP3



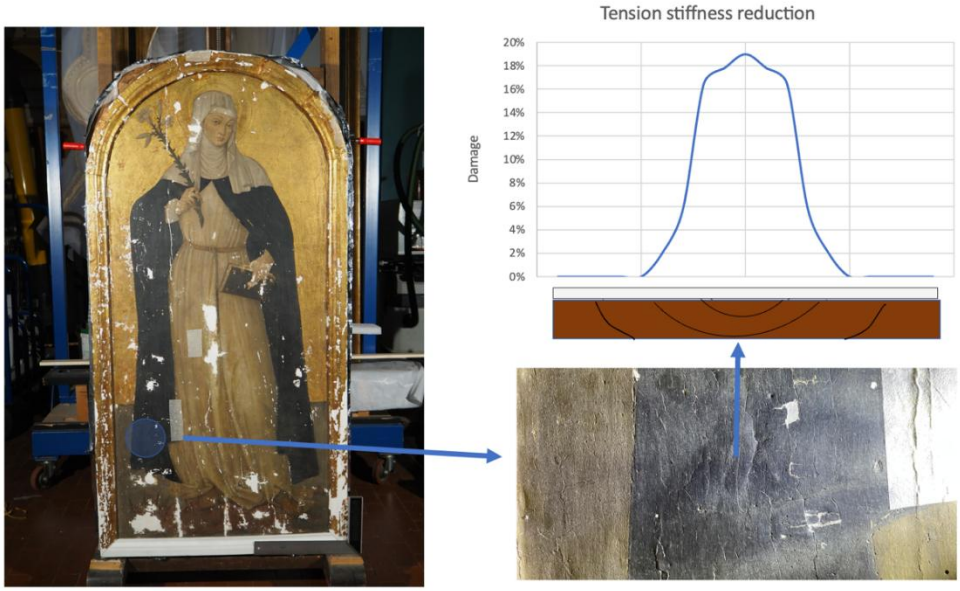


Figure 7. ***WPP3:*** *(a) Comparison of measured and simulated moisture-induced deformation of the true left side panel of the painting; (b) photo of the painting made of four planks; (c) macrophotography showing lifted and filled areas of the paint layer in the central part of the analyzed panel; (d) distribution of stiffness reduction in the paint layer in the analyzed panel.*

Table 2. Parameters of the simulation of WPP3 behavior. Results obtained with the model not taking into account the influence of cracking of the paint layer on paint stiffness [11] are shown for comparison.

	Δmc_{damage} [pp]	D_0 [$m^2 \cdot s^{-1}$]	$E_{p,high}$ [MPa]	E_{c1} [$m \cdot s^{-1}$]	X wp	Y
WPP3 old	x	$1.6\ 10^{-08}$	11470	$5.0\ 10^{-08}$	0.51	0.93
WPP3 damage	3.0	$1.5\ 10^{-08}$	11890	$5.1\ 10^{-08}$	0.56	0.96

Figure 7 shows that the model successfully reproduces the subtle asymmetry observed in WPP3, capturing the slightly different transient behavior during adsorption and desorption. The results indicate existence of the ZSL in the range of 53–60% RH. In the case of WPP3, the cracking of the paint layer results from $\Delta mc_{damage} = 3$ (Table 2). These results are remarkably consistent with those for WPP1, despite the very different mechanical properties of the two paintings ($E_0 = 11{,}890$ MPa for WPP3 compared with $E_0 = 1{,}854$MPa for WPP1). Also, in the case of WPP3, visual inspection confirms that stiffness reduction in the central part of the analyzed panel (Figure 7(d)) correlates with accumulation of damage in the paint layer (Figure 7(c))

3.3 WPP6

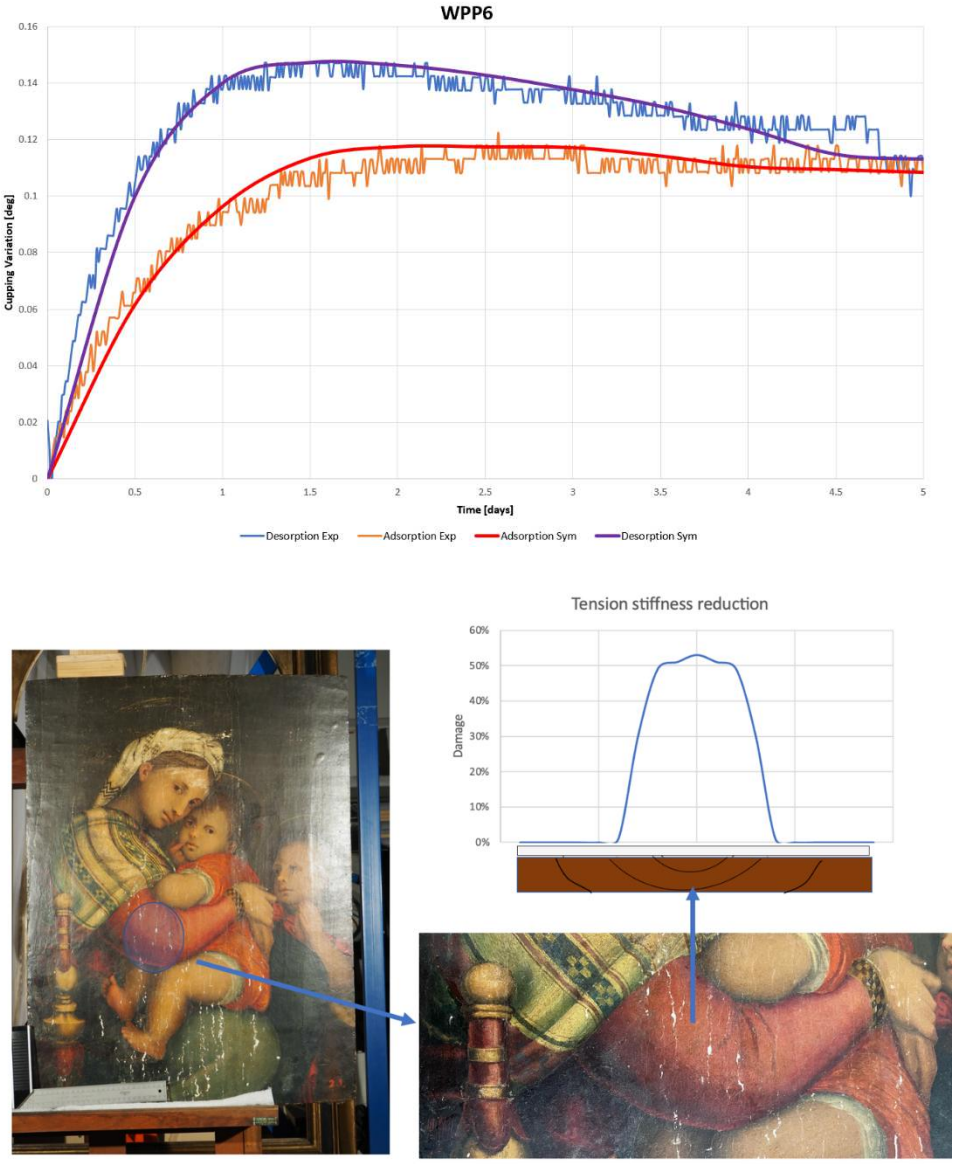


Figure 8. ***WPP6:*** *(a) Comparison of measured and simulated moisture-induced deformation of the central panel of the painting; (b) photo of the painting made of three planks; (c) macrophotography showing cracks as well as lifted and filled areas of the paint layer in the central part of analyzed panel; (d) distribution of stiffness reduction in the paint layer in the analyzed panel.*

Table 3. Parameters of the simulation of WPP6 behavior. Results obtained with the model not taking into account influence of cracking of paint layer on paint stiffness [11] are shown for comparison.

	Δmc_{damage} [pp]	D_0 [$m^2 \cdot s^{-1}$]	$E_{p,high}$ [MPa]	E_{c1} [$m \cdot s^{-1}$]	X wp	Y
WPP6 old	x	$9.0\ 10^{-10}$	563	$5.0\ 10^{-07}$	0.67	0.45
WPP6 damage	3.9	$3.2\ 10^{-10}$	703	$8.2\ 10^{-07}$	0.51	0.84

The pronounced asymmetry in WPP6 behavior is well captured by the model (Figure 8), clearly indicating a zero-stress level within the 53–60% RH range. The cracking of the paint layer results from $\Delta mc_{damage} = 3.9$ (Table 3). The undamaged paint layer modulus is $E_0 = 703$MPa, the lowest of the three. As in the cases of **WPP1** and **WPP3**, the paint layer damage in **WPP6** is mostly concentrated in the central part of the analyzed panel, correlating closely with the stiffness reduction shown in Figure 8(d).

3.4 WPP2, WPP4, WPP5

These three paintings show no difference in their response during the adsorption and desorption phases of the humidity cycle. Accordingly, damage-induced changes in the stiffness of the paint layer were not observed within the 53–60% RH range. This may indicate either that the ZSL lies outside the tested RH range or that the mechanism responsible for stiffness changes is absent or insufficient to produce a measurable effect, even if the ZSL falls within this RH range.

Because no asymmetry in the dimensional response was observed, the full damage model presented here was not applied. A simpler elastic model without damage activation provides an adequate representation of the observed behavior. The results, previously presented in [11], are included here for completeness and for comparison with the results for WPP1, WPP3, and WPP6 in Table 4.

Table 4 Simulation parameters for WPP2, WPP4, and WPP5. Results obtained using a model that does not account for the influence of paint-layer cracking on paint stiffness, reproduced from [11].

Parameter	***WPP2***	***WPP4***	***WPP5***
D_0 [$m^2 \cdot s^{-1}$]	4.5×10^{-9}	6.0×10^{-10}	1.1×10^{-9}
Ep [MPa]	2610	10500	1950
Ec [$m \cdot s^{-1}$]	4.0×10^{-8}	3.0×10^{-8}	1.0×10^{-10}
Ec1 [$m \cdot s^{-1}$]	1.1×10^{-7}	1.8×10^{-7}	2.6×10^{-7}
X	0.30	2.20	1.27
Y	0.57	1.50	0.55

3.5 Correlation between deep cracks and detection of ZSL

The obtained results confirm that deep cracks in the decorative layer of historical panel paintings act as mechanical discontinuities, opening under tension and closing under compression, which leads to asymmetry between adsorption and desorption responses. This behavior directly reflects the ZSL and that transition between tensile and compressive states in a cracked paint layer can be identified through non-invasive deformation monitoring.

Moreover, a systematic correlation was observed between the detection of ZSL and the presence of deep cracks. Following the terminology introduced in Section 2.2, the asymmetric paintings (WPP1, WPP3, WPP6) exhibit deep cracks — running along the grain and accompanied by lifting and by filled losses — while the symmetric paintings (WPP2, WPP4, WPP5) display only surface craquelure over an intact ground. These cracks are historical: they were already present, and had already been treated, when the paintings entered the OPD storage, and the mild RH cycling of the tests did not alter them; their causes are multiple and specific to each object — the climatic and mechanical history of the painting and the features of its support — and are not the subject of this study. The cracks (Figure 9 left) concentrate in areas where the panel is tangentially cut; the surface craquelure also visible there belongs to a different mechanism and plays no role in the asymmetry. A detailed description of the conservation state of the six paintings, with photographs and microscope images, is provided in the Supplementary Material.



Figure 9 – Deep cracks (left, WPP3, ZSL detected): cracks along the grain with lifted and filled paint; surface craquelure over an intact ground (right, WPP2, ZSL not detected).

Symmetric paintings (WPP2, WPP4, WPP5) exhibit uniform shallow craquelure patterns without preferred orientation confined to upper paint and varnish layers with intact ground layer, as shown in Figure 9 right. The intact ground layer explains the absence of detectable asymmetry in panels response to RH cycling. Craquelure, however conspicuous, is therefore not what the method detects: what governs stress transfer is the presence of deep cracks, which may be barely visible at the surface or concealed by fills and retouching; deformation monitoring, interpreted through the model, detects them regardless of their appearance. These observations are not intended as a general account of how and why cracks form in panel paintings, which depends on materials, construction, restraint and climatic history in ways specific to each object. They are offered as the explanation of a specific experimental evidence — the asymmetry between adsorption and desorption in three of the six paintings — and of its correlation with the presence of deep cracks.

4. CONCLUSIONS

Analysis of the experimental data of six historical Florentine panel paintings combined with inverse identification methods has provided experimental evidence of the existence of the ZSL. In the artworks exhibiting this behaviour, the stress-free state corresponds to the average relative humidity to which they have been exposed over the years, most likely during the most recent decades of their history in the OPD storage.

Three of six paintings exhibit asymmetry between adsorption and desorption responses, that can only be explained by a change in a decorative layer stiffness at ZSL. Analysis of computational modeling correlates with the observed deep cracks in the decorative layer. This holds whatever the origin of the cracks — climatic cycling, rigid restraint systems and past interventions, handling, defects at the interfaces — since what governs the response is the resulting stiffness asymmetry. In this sense the six cases explain a specific experimental evidence; they are not a general account of how and why cracks form in panel paintings. The remaining three paintings exhibit symmetric behavior, which neither confirms nor excludes the presence of a ZSL within the framework of the applied methodology.

The conditions under which ZSL occurred in 3 of the 6 paintings, despite their differences and varying environmental histories, are essentially the same and fall within the range of 53% to 60% relative humidity. This humidity range is consistent with the long-term storage environment in which the paintings have been kept. These results provide the first quantitative evidence of object adaptation, often referred to as the "acclimatization process". The cracks that make the ZSL observable are historical, formed under the uncontrolled climates and rigid restraint systems of the paintings' past, long before their current storage. Acclimatization does not require new damage: the existing cracks provide the compliance, and the time spent in a stable environment lets the stress-free state settle, through the relaxation mechanisms recalled in the Introduction, at the moisture content corresponding to the long-term average RH. Adaptation, in other words, is the condition in which the painting benefits from the cracks accumulated over its past history, which now prevent further damage. More specifically, it represents a mechanism that the object has developed to dissipate energy, making it better adapted to the changes it has undergone in the past.

This has important implications for collection management: paintings acclimatize to the environments in which they are stored over long periods and may therefore exhibit increased risk when relocated to different environments, even when the new conditions are considered superior according to standard conservation criteria.

Finally, the confirmation of ZSL and its correspondence to long-term average climatic conditions validates the "silent assumption" that objects remain in a stress-free state under long-term environmental conditions. This assumption is widely used in analyses of climate-induced mechanical damage risk, which constitutes a cornerstone of risk assessment for museum collections and is the foundation of museum environmental guidelines. The finding that the conditions at ZSL, where these have been established, correspond to long-term average climatic conditions, appears to provide confirmation of the premise that objects can reach a stress-free state under stable long-term environmental conditions. This assumption, if confirmed by further essential experimental evidence, could usefully be incorporated into analyses of the risk of climate-induced mechanical damage, which constitute a fundamental pillar of risk assessment for museum collections and form the basis of museum environmental guidelines.

CRediT authorship contribution statement

Lorenzo Riparbelli: Conceptualization; Methodology (overall methodological approach and technical development, including the mechanical framework, numerical modelling and experimental design); Software; Investigation; Formal analysis (experimental data analysis, numerical analyses and parameter identification); Validation; Visualization; Funding acquisition; Writing – original draft (including scientific framing); Writing – review & editing.
Łukasz Bratasz: Conceptualization; Validation; Writing – review & editing.
Michał Łukomski: Conceptualization; Validation; Writing – original draft; Writing – review & editing.
Paola Mazzanti: Investigation (experimental testing); Methodology (experimental design); Formal analysis (experimental data analysis); Writing – review & editing.
Luciano Ricciardi, Sandra Rossi, Ciro Castelli and Andrea Santacesaria: Resources (access

to the paintings); Investigation (examination and conservation assessment of the paintings); Methodology (guidance on the experimental approach, experimental design); Supervision (experimental work at the Opificio delle Pietre Dure); Writing – review & editing.
Marco Fioravanti: Conceptualization; Methodology (overall methodological approach); Validation; Research coordination; Writing – review & editing.

Declaration of competing interest

The authors declare that they have no known competing financial interests or personal relationships that could have appeared to influence the work reported in this paper.

Data availability

Data will be made available on request.

Funding

This research was funded by the European Union's Horizon Europe research and innovation programme under the Marie Skłodowska-Curie Actions grant agreement No. 101155233 (MASTERPIECE; Lorenzo Riparbelli). Funded by the European Union. Views and opinions expressed are, however, those of the author(s) only and do not necessarily reflect those of the European Union or the European Research Executive Agency (REA). Neither the European Union nor the granting authority can be held responsible for them.

Bibliography

1. Mecklemburg M (1991) Art in transit. 1: Studies in the transport of paintings. Washington
2. Erhardt D, Mecklenburg M (1994) Relative humidity re-examined. Studies in conservation 39(sup2):32–38
3. Mecklenburg M, Tumosa C, Erhardt D (1998) Structural response of painted wood surfaces to changes in ambient relative humidity. In: Painted Wood: History and Conservation, The Getty Conservation Institute. Dorge V. and Howlett FC, US, pp 464–483
4. Michalski S (1991) Paintings, their response to temperature, relative humidity, shock and vibration. National Gallery London, UK
5. Ciatti M, Frosinini C (2016) Structural conservation of panel paintings at the Opificio delle Pietre Dure in Florence: method, theory, and practice. Edifir Edizioni Firenze, Florence (Italy)
6. Ciatti M (2013) Per la conservazione dei dipinti: esperienze e progetti del Laboratorio dell'OPD (2002 - 2012); atti della Giornata di Studi in occasione degli 80 anni del Laboratorio di restauro dei dipinti mobili (1932 - 2012) del 5 dicembre 2012 (Firenze, Auditorium di Sant'Apollonia). Edifir, Firenze
7. (1998) The structural conservation of panel paintings. In: Proceedings of a Symposium at the J. Paul Getty Museum 24-28 April 1995. Dardes K. and Rothe A., The Getty Conservation Institute, US

8. Getty Foundation (2018) The Getty Foundation Panel Paintings Initiative - Final report. Getty Foundation, Los Angeles US
9. Bratasz Ł (2013) Allowable microclimatic variations for painted wood. Studies in Conservation 58:65–79. https://doi.org/10.1179/2047058412Y.0000000061
10. Rachwał B, Bratasz Ł, Łukomski M, Kozłowski R (2012) Response of Wood Supports in Panel Paintings Subjected to Changing Climate Conditions. Strain 48:366–374. https://doi.org/10.1111/j.1475-1305.2011.00832.x
11. Riparbelli L, Mazzanti P, Helfer T, Manfriani C, Uzielli L, Castelli C, Santacesaria A, Ricciardi L, Rossi S, Gril J, Fioravanti M (2023) Modelling of hygro-mechanical behaviour of wooden panel paintings: model calibration and artworks characterisation. Herit Sci 11:126. https://doi.org/10.1186/s40494-023-00958-9
12. Riparbelli L, Mazzanti P, Manfriani C, Uzielli L, Castelli C, Gualdani G, Ricciardi L, Santacesaria A, Rossi S, Fioravanti M (2023) Hygromechanical behaviour of wooden panel paintings: classification of their deformation tendencies based on numerical modelling and experimental results. Herit Sci 11:25. https://doi.org/10.1186/s40494-022-00843-x
13. Michalski S (2007) The Ideal Climate, Risk Management, the ASHRAE Chapter, Proofed Fluctuations, and Toward a Full Risk Analysis Model. Risk Management
14. Bratasz Ł, Vaziri Sereshk MR (2018) Crack Saturation as a Mechanism of Acclimatization of Panel Paintings to Unstable Environments. Studies in Conservation 63:22–27. https://doi.org/10.1080/00393630.2018.1504433
15. Ciatti M (2006) Panel painting: technique and conservation of wood supports, Rev. English ed. Edifir, Firenze
16. Mecklenburg MF (2011) Determining the acceptable ranges of RH and T in museums and galleries, Part 1. Museum Conservation Institute, the Smithsonian Institution
17. Hagan EWS (2017) Thermo-mechanical properties of white oil and acrylic artist paints. Progress in Organic Coatings 104:28–33. https://doi.org/10.1016/j.porgcoat.2016.10.019
18. Gril J, Jullien D, Hunt D (2016) Compression set and cupping of painted wooden panels. In: Analysis and Characterisation of Wooden Cultural Heritage by Scientific Engineering Methods. Halle (Saale), Germany
19. Hunt D (1992) Present knowledge of mechano-sorptive creep of wood, Creep in Timber Constructions (a state of the art report). Rilem Technical Committee 112:75–104
20. ASHRAE ASHRAE [American Society of Heating, Refrigerating, and Air-Conditioning Engineers]., Museums, Galleries, Archives, and Libraries. Chap 24 in ASHRAE Handbook—HVAC Applications, vol. 4, 4 voll. Atlanta, USA: ASHRAE [American Society of Heating, Refrigerating, and Air-Conditioning Engineers]., 2019
21. EN 15757:2010 «EN 15757:2010 - Conservation of Cultural Property - Specifications for temperature and relative». https://standards.iteh.ai/catalog/standards/cen/ad03d50b-22dc-4c57-b198-2321863f3870/en-15757-2010
22. Camuffo D, Della Valle A, Becherini F (2022) The European Standard EN 15757 Concerning Specifications for Relative Humidity: Suggested Improvements for Its Revision. Atmosphere 13:1344. https://doi.org/10.3390/atmos13091344
23. Riparbelli L, Mazzanti P, Helfer T, Manfriani C, Uzielli U, Castelli C, Santacesaria A, Ricciardi L, Rossi S, Gril J, Fioravanti M (2024) Exploring the inner hygro-mechanical behaviour of historical panel paintings: a novel approach using digital twins. Herit Sci 12:27. https://doi.org/10.1186/s40494-023-01106-z

24. Uzielli L, Cocchi L, Mazzanti P, Togni M, Julien D, Dionisi-Vici P (2012) The Deformometric Kit: A method and an apparatus for monitoring the deformation of wooden panels. Journal of Cultural Heritage 13:94–101
25. Krzemień L, Łukomski M, Bratasz Ł, Kozłowski R, Mecklenburg MF (2016) Mechanism of craquelure pattern formation on panel paintings. Studies in Conservation 61:324–330. https://doi.org/10.1080/00393630.2016.1140428
26. Hagan EWS (2017) Thermo-mechanical properties of white oil and acrylic artist paints. Progress in Organic Coatings 104:28–33. https://doi.org/10.1016/j.porgcoat.2016.10.019
27. Stöcklein J, Konopka D, Grajcarek G, Tietze O, Oertel S, Schulze A, Kaliske M (2022) Hygro-mechanical short-term behaviour of selected coatings: experiments and material modelling on vapour permeability and mechanical properties. Herit Sci 10:141. https://doi.org/10.1186/s40494-022-00768-5
28. Bucklow S (2020) The classification of craquelure patterns. In: Stoner JH, Rushfield R (eds) Conservation of Easel Paintings, 2nd ed. Routledge, pp 295–301
29. Lorenzo R, Paola M, Thomas H, Chiara M, Luca U, Ciro C, Andrea S, Luciano R, Sandra R, Joseph G, Marco F (2024) Exploring the inner hygro-mechanical behaviour of historical panel paintings: a novel approach using digital twins. Herit Sci 12:27. https://doi.org/10.1186/s40494-023-01106-z
30. Riparbelli L, Dionisi-Vici P, Mazzanti P, Brémand F, Dupré JC, Fioravanti M, Goli G, Helfer T, Hesser F, Jullien D, Mandron P, Ravaud E, Togni M, Uzielli L, Badel E, Gril J (2023) Coupling numerical and experimental methods to characterise the mechanical behaviour of the Mona Lisa: a method to enhance the conservation of panel paintings. Journal of Cultural Heritage 62:376–386. https://doi.org/10.1016/j.culher.2023.06.013
31. Helfer T, Wangermez M, Simo E, Nagel T, Silbermann CB, Riparbelli L (2025) The MFrontGallery project. JOSS 10:7742. https://doi.org/10.21105/joss.07742
32. EDF - Électricité De France (2022) Finite element Code_Aster: Analyse des Structures et Thermo-mécanique pour des Etudes et des Recherches
33. Helfer T, Michel B, Proix J-M, Salvo M, Sercombe J, Casella M (2015) Introducing the open-source mfront code generator: Application to mechanical behaviours and material knowledge management within the PLEIADES fuel element modelling platform. Computers & Mathematics with Applications 70:994–1023. https://doi.org/https://doi.org/10.1016/j.camwa.2015.06.027
34. Rachwał B, Bratasz Ł, Krzemień L, Łukomski M, Kozłowski R (2012) Fatigue Damage of the Gesso Layer in Panel Paintings Subjected to Changing Climate Conditions. Strain 48:474–481. https://doi.org/https://doi.org/10.1111/j.1475-1305.2012.00844.x
35. Mastorakis NE (2005) On the solution of ill-conditioned systems of linear and non-linear equations via genetic algorithms (GAs) and Nelder-Mead simplex search. In: Proceedings of the 6th WSEAS international conference on Evolutionary computing. World Scientific and Engineering Academy and Society (WSEAS), Stevens Point, Wisconsin, USA, pp 29–35
36. Assimi H, Jamali A (2018) A hybrid algorithm coupling genetic programming and Nelder–Mead for topology and size optimization of trusses with static and dynamic constraints. Expert Systems with Applications 95:127–141. https://doi.org/10.1016/j.eswa.2017.11.035

Annex A – Diffusion model and finite element discretisation

To simulate moisture diffusion in a painting, we employed an isotropic model based on Fick's law in its time-dependent form:

$$\frac{\partial m_c}{\partial t} = \nabla \cdot \left(\underline{\boldsymbol{D}} \cdot \nabla m_c\right) \qquad \text{Equation 1}$$

where:

- $\boldsymbol{m_c}$ is the moisture content, defined as $\boldsymbol{m_c} = \frac{m - m_0}{m_0}$, with m representing the current mass of the wood and m0 the dry mass.
- $\underline{\boldsymbol{D}}$ is the diffusion coefficient tensor, representing the rate of moisture diffusion through the wood.
- $\boldsymbol{\nabla}$ denotes the gradient operator, used here to describe the spatial variation of moisture content.

For computational efficiency, the diffusion coefficient tensor $\underline{\boldsymbol{D}}$ is simplified to an isotropic form as:

$$\underline{\boldsymbol{D}} = \begin{bmatrix} \boldsymbol{D_0} \\ \boldsymbol{D_0} \\ \boldsymbol{D_0} \end{bmatrix} \qquad \text{Equation 2}$$

where D_0 [mm²/s] is the isotropic moisture diffusion coefficient.

The boundary condition used to model the paint layer's emissivity is total insulation to moisture transfer.

To model the rear wooden face of the panel, we used the following boundary condition:

$$\frac{q_r}{\rho_0} = E_{c1} \cdot \left(m_{r,air} - m_{r,sur}\right) \qquad \text{Equation 3}$$

where:

- q_r [Kg×s^{-1}×m^{-2}] is the total moisture flux at the paint boundary.
- $\boldsymbol{\rho_0}$ [Kg×m^{-3}] is the wood density in dry conditions
- $\mathbf{E_{c1}}$ [m×s^{-1}] is the global moisture effective emissivity of the rear wood surface.
- $\boldsymbol{m_{r,air}}$ and $\boldsymbol{m_{r,sur}}$ are the wood's equilibrium moisture content corresponding to air humidity and the moisture content immediately below the rear face, respectively.

In our computational study, we utilised different finite element types to optimise accuracy and computational efficiency for various analysis aspects. For hygroscopic analysis, we used first-order hexahedral finite elements, essential for capturing moisture changes in the cross section. For mechanical computations, we employed second-order hexahedral finite elements for the panel, providing a higher precision in capturing stress distributions and deformations. At each computational step, the hygroscopic field was projected onto the mechanical mesh. The mechanical behaviour of the wood was modelled using a homogeneous orthotropic linear elastic framework in cylindrical coordinates, with the pith as the central reference point. This model also accounted for material shrinkage and swelling in the same cylindrical coordinate system.

Annex B – Constitutive law ENDO_LOCA_TC and calibration

To capture this behaviour, the paint layers are modelled using the ENDO_LOCA_TC constitutive law implemented in code_aster [32]. This model is the result of over 25 years of progressive development at EDF, aimed at constructing a hierarchy of damage models with increasingly rich phenomenology while maintaining numerical robustness [EDF Technical documentation].

The law of behavior ENDO_LOCA_TC was specifically developed to address the need for a model that combines:

- **Numerical robustness**: essential for iterative inverse identification procedures involving hundreds of simulations
- **Unilateral damage effect**: different stiffness degradation in tension versus compression
- **Distinct initiation thresholds**: separate damage onset criteria for tensile and compressive loading
- **Bounded stress response**: finite strength limits in both tension and compression

The model is isotropic, local (no non-local regularisation required for the present application), and does not introduce irreversible strains—appropriate for quasi-brittle materials.

Two characteristics of ENDO_LOCA_TC make it particularly suitable for modelling cracked paint layers:

- **Snap-back behaviour in tension**. Immediately after reaching the tensile strength, the model exhibits a sharp stress drop (snap-back) followed by gradual softening. This abrupt post-peak response is characteristic of brittle and quasi-brittle materials where crack propagation is sudden rather than progressive. For paint layers, this behaviour is physically realistic: once the tensile strength of the gesso and/or paint film is exceeded, fracture occurs rapidly with minimal additional energy dissipation, producing the sharp-edged cracks observed in historical craquelure.
- **Stiffness restoration upon crack closure**. The model incorporates a parameter η controlling the degree of stiffness recovery when the material transitions from tension to compression. When $\eta \rightarrow 1$, the model recovers nearly complete compressive stiffness despite prior tensile damage. This captures the essential physics of crack closure: the fractured surfaces come back into contact and can transmit compressive loads, while remaining unable to sustain tension.

The model introduces a tensile damage variable $a \in [0,1]$ and a compressive damage variable c. The effective Young's modulus depends on the loading direction:

- Under tension: $E_t = A(a) \cdot E_0$
- Under compression: $E_c = C(c) \cdot E_0$

where E_0 is the modulus of undamaged material and A(a), C(c) are degradation functions satisfying $A(0) = C(0) = 1$ (intact material). The function A(a) decreases monotonically with damage accumulation, while C(c) incorporates the stiffness restoration mechanism.

The mechanical properties of historical paint layers cannot be reliably determined from literature data on modern materials. The specific fracture energy, crack spacing, and softening characteristics of a multi-century-old gesso-paint stratigraphy are unknown and imposible to determine through direct measurement without destructive testing..

We therefore adopt a **phenomenological calibration** approach: rather than attempting to assign physically "correct" values to material parameters, we calibrate the model to reproduce mechanical response consistent with the observed behaviour of cracked paint layers. The calibration is defined by four criteria:

1. **Criterion 1 — Damage initiation threshold ($\varepsilon_0 = 0.2\%$)**

The tensile strength ft is set such that damage initiates at a strain of 0.2% [34].

With E_0 identified through optimisation, this criterion yields $f_t = E_0 \times 0.002$.

2. **Criterion 2 — Abrupt post-peak collapse (snap-back)**

The softening exponent p is set to a value less than unity ($p < 1$), which produces an immediate sharp stress drop after reaching the tensile strength. This snap-back response represents:

- The brittle nature of gesso and aged paint films
- Rapid crack propagation once the strength threshold is exceeded
- Minimal energy dissipation in the fracture process

This is in contrast to ductile materials ($p > 1$) where the post-peak stress decreases gradually.

3. **Criterion 3 — Residual stiffness at reference strain (2% at $\varepsilon = 0.5\%$)**

The combination of fracture energy GF, characteristic length Lf, and softening exponent p is calibrated such that at $\varepsilon = 0.5\%$ [27], the damaged material retains only 2% of its original stiffness. This severe degradation represents:

- A fully developed crack state where the paint layer offers minimal resistance to further opening
- A reference point within the hygroscopic strain range of interest
- Numerical stability (non-zero residual stiffness prevents ill-conditioning)

4. **Criterion 4 — Near-complete stiffness restoration ($\eta \approx 1$)**

The crack closure parameter is set to $\eta = 1$, representing near-total recovery of compressive stiffness when cracks close. This assumption reflects:

- The morphology of age cracks, which typically present clean, interlocking fracture surfaces
- The absence of debris or permanent deformation in the crack void
- The reversible nature of the asymmetric response observed experimentally

5. **Criterion 5 — Compression damage disabled**

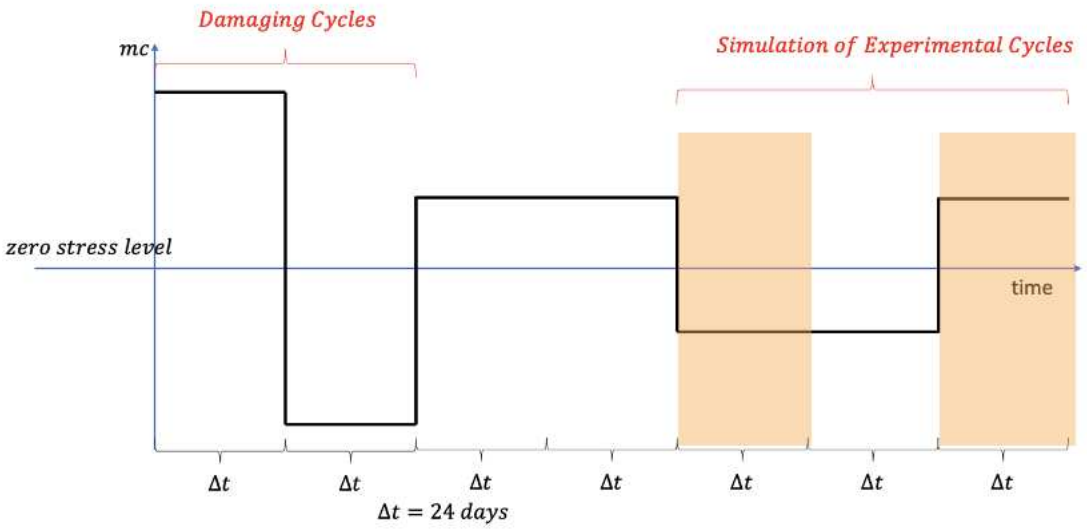
The compressive strength fc and onset threshold σ_0 are set to values sufficiently high that compression damage never activates within the strain range of interest. This reflects the physical observation that historical paint layers exhibit cracking (tensile damage) but not crushing (compressive damage) under hygroscopic loading.

The damage parameters are defined in terms of strain thresholds rather than stress thresholds. This choice reflects the impossibility of determining actual paint layer thickness without invasive sampling. The model employs a nominal thickness of 0.5 mm; consequently, the optimisation identifies the product E × t (extensional rigidity) rather than E alone, considering that the thickness of the paint layers is negligible compared to the total thickness of the artworks [23, 11].

For deformation predictions this ambiguity is inconsequential - curvature depends on extensional rigidity, not on E and t independently. For stress predictions, however, thickness uncertainty propagates directly into error. To maintain consistency, the formulation is expressed entirely in strain terms: damage initiates at $\varepsilon_0 = 0.2\%$, calibration targets residual stiffness at reference strain (2% at $\varepsilon = 0.5\%$). This approach ensures that identified quantities remain valid regardless of thickness uncertainty.

Annex C – Sensitivity analysis and parameter degeneracy

The sensitivity analysis from [11] applies directly to the present damage-based formulation. The optimisation includes six parameters: D_0, Ec_1, Ep, X, Y and Δmcdamage. The first five retain their definitions and their relationships with the measured deformation from [11]. The additional parameter, Δmcdamage, controls the damage field through the amplitude of the fictitious damaging cycle. Its influence on deformation is confined to the decorative-layer stiffness when cracks are open, which decreases monotonically as Δmcdamage increases; Ep defines the stiffness when cracks are closed. Δmcdamage therefore enters the identification as a stiffness variable. The sensitivity and distinguishability established in [11] for paint-layer stiffness consequently apply to this parameter, provided that damage has not saturated. The non-uniform damage fields in Figures 6d, 7d and 8d confirm that this condition holds for the identified values. The sensitivity study demonstrating well-posedness and parameter distinguishability transfers without modification.



The fictitious damaging cycles used to generate the initial damage state are centred on the midpoint of the experimental humidity range (56% RH). This assumption is necessary because the experimental protocol—a single cycle between 53% and 60% RH—does not provide sufficient information to independently identify both the ZSL position and the no-damage range amplitude. The physical basis for this limitation is as follows. The measured asymmetry between adsorption and desorption depends on when the stiffness transition occurs during the humidity cycle, which is governed by the ZSL position, and on how much stiffness contrast exists between crack-open and crack-closed states, which is governed by the damage severity and hence by ΔMC_damage. Within a single experimental cycle, a shift in ZSL position can be partially compensated by an adjustment in ΔMC_damage, producing nearly equivalent deformation responses. This parameter degeneracy cannot be resolved without additional experimental information—for instance, cycles of different amplitude or mean humidity. By fixing ZSL at the interval midpoint, the optimisation identifies ΔMC_damage values that absorb any actual deviation from this assumption. The resulting uncertainty in ZSL position is bounded by half the experimental range: if detectable asymmetry exists, ZSL must lie within the 53–60% RH window, and the maximum error from assuming the central value is cautionsly ±5% RH also considering the margin from 10% sensitivity range. The identified no-damage ranges should be interpreted with corresponding uncertainty of approximately ±5% RH in their absolute position, although their amplitude remains well-constrained by the optimisation.

Supplementary Files

This is a list of supplementary files associated with this preprint. Click to download.

- SupplementaryMaterial.docx